nature reviews materials

https://doi.org/10.1038/s41578-026-00915-5

Review article

Check for updates

Inverse design for scalable photonic systems

Louise Schul[1,2], Sydney Mason[1,2], Sungjun Eun[1,2], Geun Ho Ahn[1,2] & Jelena Vučković[1,2]

Abstract

Over the past two decades, photonic inverse design has emerged as a powerful approach to implement photonic devices with improved performance or to realize new functionalities. Whereas the efforts over the first decade focused on proof-of-concept devices designed and fabricated in university laboratories, the focus over the past 5–10 years has shifted towards implementation of scalable photonic systems. This Review surveys this recent progress and the challenges and new directions in photonics inverse design. We focus on large-scale 3D photonic inverse design, including metasurfaces, on the translation of inverse design to commercial foundries and practical silicon photonics, on the application of photonic inverse design to different materials systems, wavelengths and optical effects and, finally, on new directions such as inverse design of quantum systems.

Sections

[1]Department of Electrical Engineering, Stanford University, Stanford, CA, USA. [2]Ginzton Laboratory, Stanford University, Stanford, CA, USA. e-mail: jela@stanford.edu

Introduction

Photonic inverse design is an approach in which photonic devices are designed by defining desired input-to-output optical field mapping and then by efficiently searching through the full parameter space to find the geometry that satisfies the desired functionality with any additional imposed constraints (such as fabrication, environment, bandwidth or efficiency)[1,2]. For nearly all photonics problems of interest, this search has to be performed in a 3D parameter space to accurately capture and describe the device performance. Because the parameter space is enormous even for modest footprint devices, blind search is impossible, and physics-guided search is crucial. For example, the use of 20-nm binary pixels for a 3D device with a linear dimension of 2 μm leads to $2^{1,000,000}$ possibilities — more than the number of atoms in the observable universe. Physics-guided search means gradient descent towards a local optimum through this complex parameter space, by calculating spatial gradients to the figure of merit that is being optimized. Because gradient calculation is computationally very expensive, this process is done by adjoint optimization, which is mathematically very similar to backpropagation. Adjoint optimization computes full spatial gradients in devices with only two full-wave simulations per iteration: a forward simulation with the expected input excitation, and an adjoint (backward) simulation with a source constructed from the desired output, exciting the structure backwards.

Using a simple mathematical trick, structure gradients can be calculated from these two simulations (Fig. 1), allowing us to update the structure in the way that would lead to the local optimum[1,2]. This process is typically repeated several hundreds of times until a local optimum that satisfies requirements and constraints is found, requiring several hundreds of electromagnetic simulations to be done in series (two per step). Because electromagnetic simulations are generally slow and computationally expensive, especially for 3D devices, one of the main challenges and goals in photonic inverse design is the development of fast electromagnetic simulators, which are scalable to large 3D footprints[3]. Further complicating this process is the fact that for practical devices, optimization is constrained (binary structure, minimum feature sizes, large bandwidth and so on).

This Review surveys recent progress, challenges and new directions in photonics inverse design, focusing on the developments reported since the previous extensive review of the field in 2018 (ref. 1). In particular, we focus on what we believe are the main recent developments: large-scale 3D photonic inverse design, including metasurfaces; translation of inverse design to commercial foundries and practical silicon photonics; application of photonic inverse design to different materials systems, wavelengths and optical effects (including nonlinear); and finally, new directions in photonic inverse design, in particular in nonlinear optical and quantum systems. Figure 2 shows an overview of these developments.

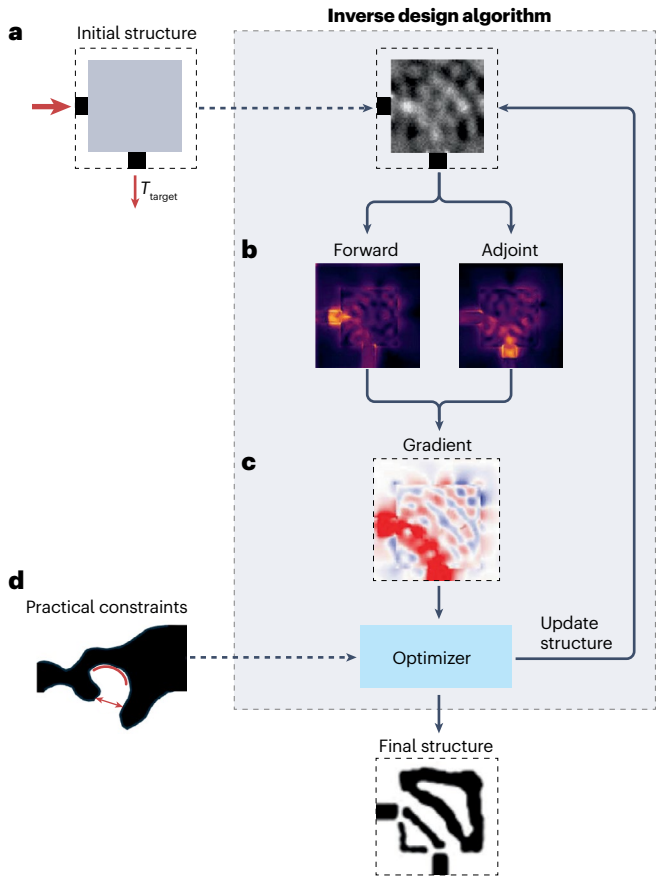

Fig. 1 | Photonics inverse design of a waveguide bend via adjoint optimization. **a**, The structure is initialized as a black box with fixed footprint and desired transmission efficiency (T_{target}). **b**, The structure gradient is calculated from two electromagnetic simulations: forward and backward (adjoint). This process is similar to backpropagation in artificial intelligence. **c**, Gradient descent efficiently searches through the parameter space. **d**, Practical devices require constraints such as binary structure and minimum feature sizes.

Large-scale photonics inverse design

As electromagnetic solvers have advanced[3–5], inverse design has become pervasive in fields that are historically constrained by simulation size, such as free-space optics. Metasurfaces are typically made up of a periodic array of subwavelength-scale structures, the meta-atoms, and can manipulate all the properties of light at the nanoscale, providing new functionalities for free-space beam control and a more efficient and miniaturized alternative to bulk optic components. Enabled by larger simulation regions and creative approximation techniques, there has been a recent explosion of inverse design of metasurfaces. A variety of methods have been explored to exploit inverse-design concepts[6,7] and depart from the traditional manual parameter tuning and iterative brute-force search design method that has been used for decades. For the purpose of categorizing inverse-design regimes by simulation size, we define large-scale inverse design as bigger than 20 μm × 20 μm (or ~50λ/n and larger in linear dimension), medium-scale around 10–20 μm, and small-scale as smaller than 10 μm. Owing to the dominance of metasurfaces in existing work on large-scale inverse design, in this section, we mainly focus on metasurface design approaches.

For the inverse design of metasurfaces, three main approaches have emerged. The simulation of a single meta-atom required for building a library of shapes is not computationally expensive. However, even with this pre-existing library, the design of large-area metasurfaces has been limited by the computational power required to calculate the desired phase profile. The state-of-the-art approach for the inverse design of a metasurface phase profile uses a combination of a fast approximate solver for far-field calculations and the adjoint method to design and experimentally demonstrate meta-optics with sizes on the order of 20,000λ (ref. 8) (Fig. 2a). In this approach, a training set of meta-atoms and their simulated field response were used to predict the local field of an arbitrary meta-atom. Designing

a metasurface with multiple outputs is computationally infeasible with classical approaches but possible with inverse design. For example, it is possible to encode nine holograms into one metasurface and create 3D holograms using phase profile optimization[9], as well as use the adjoint gradient method to design an achromatic metalens doublet with a large numerical aperture, a metasurface doublet with five different wavelength-dependent holograms, and a multiple metasurface optical neural network for classifying digits[10]. This can be extended to more dimensions, enabling multichannel imaging (depth, spectral or polarization) with an inverse-designed metasurface multiplexer, spatially separating wavelengths as narrow as 20 nm apart[11] (Fig. 2b). Other approaches overcome limitations in full-wave simulation capacity by using neural networks[12,13], genetic algorithms[14] and coupled-mode theory[15,16]. These methods have been used to design large-area, high-efficiency metasurfaces in optical and THz frequencies. Notably, in many cases, using the adjoint method can result in the optimization being stuck in some non-optimal local minimum of the loss function as a result of the initial condition. To resolve this issue, an approach called GLOnet-based optimization can be utilized, which enables a global search of the design space[17].

The second approach to the inverse design of metasurfaces is topology optimization at the unit cell level. This method allows for the design of meta-atoms with unintuitive geometries that, when placed in a periodic array, perform precisely defined functions such as beam deflection and focusing at gigahertz frequencies[18], polarization filters, half-wave and quarter-wave plates[19,20], producing arbitrary spectral responses[21], and solving integral equations[22]. Most metasurface design approaches ignore inter-meta-atom coupling between meta-atoms of dissimilar shapes, which can limit performance. A shape optimization method using the Fourier decomposition of the surface gradient was developed to optimize the meta-atoms of an existing library, allowing only for fabrication-friendly smooth variations of the geometries[23].

Finally, metasurface inverse design extends beyond phase profile optimization and unit cell design and into free-form optimization of the entire surface topology. These approaches include 1D grating optimizations for large-area metasurfaces (10^4–$10^5\lambda$)[24], the design of 3D meta-optics using full-wave, finite-difference time-domain (FDTD) simulations and the adjoint method[23], and specialized solvers for full metasurfaces such as the T-matrix method[25]. The power of extending inverse design to multi-layer 3D structures has been demonstrated with a six-layer meta-optics device that sorts angular momentum and polarization, and spectrally filters in the mid-infrared[26] (Fig. 2c). Free-form metasurface inverse design has enabled new functionalities, such as complementary scanning lenses for terahertz imaging[27] and tailored spatial and spectral responses that recreate the colour perception of the human eye[28]. These demonstrations would have been infeasible with the classical unit cell approach. Even with current state-of-the-art electromagnetic solvers, free-form 2D optimization of large-area metasurfaces remains challenging. In certain design scenarios, such as a lens, there are inherent symmetries that allow for the clever avoidance of optimizing the entire metasurface. Instead, the metalens can be broken into radial zones, allowing for the full-wave simulation in cylindrical coordinates while exploiting a GPU-accelerated FDTD solver[29]. This technique facilitated the realization of a wide-aperture free-form 3D metalens[29] (Fig. 2d).

Additional applications, such as fibre couplers, can benefit from imposing radial symmetry to reduce the design region size for 3D structures. To improve the coupling efficiency between single-mode fibres and photonic wire bonds, gradient-based inverse design has been used to design 3D nanoprinted couplers[30]. This approach is used for couplers with a length of 25 µm and greater, achieving coupling efficiencies between the single-mode fibre and photonic wire bond of more than 90%. Large-area inverse design has also been leveraged for on-chip applications that require longer propagation lengths, such as mode sorting on a surface plasmon polariton platform, wherein a design region of 52 × 38 µm was used[31].

Efforts towards scaling inverse-design structures have permeated medium-scale devices such as fibre-to-chip couplers. Grating couplers were an excellent initial demonstration for inverse design, with inverse-designed 1D gratings exceeding the performance of traditional grating couplers with uniform or apodized periodicity[32]. Since these preliminary demonstrations, design regions have been expanded to a 2D area on the order of 10 × 10 µm to 14 × 14 µm to accommodate telecom fibre modes with spot sizes of ~10 µm (refs. 33–35). Coupling efficiencies of less than −3.4 dB with >60 nm 3-dB bandwidth have been realized in the O-band and C-band of telecommunications[33]. Inverse design has been shown to be a suitable solution for grating couplers for vertically incident light, which present increased design difficulty. Commercial foundry-compliant multi-layer inverse-design grating couplers have been demonstrated to achieve −4.7 dB coupling efficiency for vertically incident light[34]. This efficiency can be increased even further when a reflector is added below the grating coupler, enabling sub-decibel coupling efficiency for a 14 × 14 µm coupler[35].

Inverse-design translation to commercial foundries

Building on over a decade of proof-of-concept photonic inverse-design demonstrations[1], its natural progression to high-throughput fabrication and commercial semiconductor foundries has happened over the past 5–10 years. Commercial semiconductor manufacturing relies on photolithography processes, which have considerably lower resolutions than electron-beam lithography and ion beam machining[36]. To ensure manufacturability, foundries impose geometrical constraints, including minimum linewidth, linespacing, curvature, area and enclosed area. Designs must pass thousands of design rule checks (DRC) to be fabricated[37,38]. The inverse-design workflow for commercial foundries is illustrated in Fig. 3.

Inverse-designed devices frequently include small features that violate DRC and are, therefore, difficult or impossible to fabricate[36,37,39–44]. Moreover, inverse-designed devices are highly sensitive to minor fabrication variations, leading to performance degradation[38,39,43]. These challenges motivate inverse-design frameworks that integrate manufacturability and robustness directly into the optimization process. Strategies for robust DRC-compliant designs include imposing analytic constraints during the optimization, selecting a design parameterization that guarantees geometric feasibility, integrating lithography models into the optimization process, and using machine-learning techniques.

Imposing analytic constraints during optimization is a common strategy to guide the process towards manufacturable structures. The first successful demonstration of inverse design in a commercial silicon process incorporated heuristics for minimum feature gap and curvature into gradient-based optimization[36]. The researchers fabricated a spatial mode multiplexer, a wavelength demultiplexer (Fig. 2e), a 50–50 directional coupler, and a three-way power splitter, and they verified that all four designs were robust to fabrication errors, with ±0.6 dB device-to-device variability across three dies.

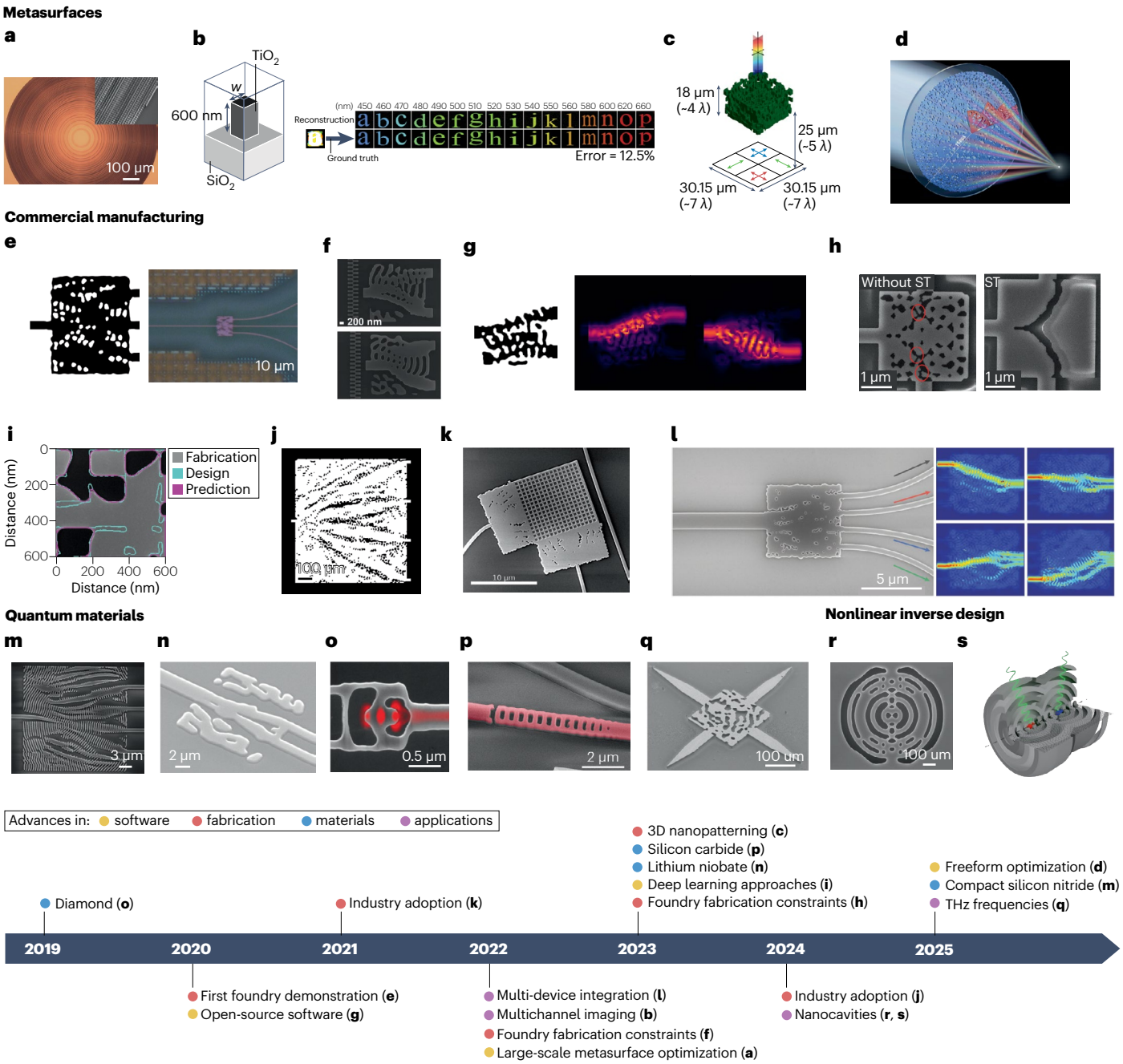

The introduction of additional 2D constraints on minimum area and enclosed area produced broadband waveguide bends, T-splitters and reflectors complying with nine different foundry specifications[38]. As an alternative to geometric constraints, imposing an energy constraint can direct the optimization process to solutions that best contain the field inside silicon[39,40,44]. This method offers three advantages: it naturally generates devices that are closer to binarized; it results in less energy interacting with boundaries and being affected by dimensional variations; and it naturally limits the generation of small features. When applied to 3D optimization for three types of devices (a mode converter, an O-band/C-band duplexer (Fig. 2f), and a C-band three-channel wavelength-division multiplexer (WDM)), the energy constraint improved binarization and reduced the presence of small features[39].

Alternatively, 'always-feasible' design methodologies select design parameterizations that guarantee manufacturability without the need for analytic constraints. Notably, topology optimization generates intermediate permittivity values that cannot be fabricated and, thus, requires a multistage optimization process. A typical workflow begins with initial optimization of a continuous permittivity distribution, followed by discretization and further optimization under fabrication constraints. When applied to a silicon-on-insulator two-channel WDM,

Fig. 2 | Progression of inverse design since 2019. **a**, Large-scale red-blue-green (RGB)-achromatic polarization-insensitive metalens (2022). **b**, Sixteen-channel metasurface spectral imager (2022). **c**, Three-dimensional-patterned multispectral and polarization sorting device (2023). **d**, Wide-aperture free-form 3D metalens (2025). **e**, Three-channel wavelength-division multiplexer (WDM) fabricated in a commercial silicon foundry (2020). **f**, Duplexer, of 1,310-nm (top) and 1,550-nm (bottom) wavelength, optimized with energy constraint (2022). **g**, Two-channel silicon-on-insulator WDM designed using the software SPINS (2020). **h**, T-Junction optimized with structure transformation (ST) (2023). **i**, Output of a deep-learning model used to predict fabrication outcomes (2023). **j**, Four-channel compact WDM designed at Google (2024). **k**, Compact dual-polarization silicon-integrated couplers for multicore fibres (2021). **l**, Four-channel broadband low-crosstalk mode division multiplexer (MDM) (2022). **m**, Four-channel compact WDM in silicon nitride (2025). **n**, Two-channel lithium niobate MDM (2023). **o**, Diamond vertical coupler (2019). **p**, Silicon carbide reflector in Fabry–Perot cavity for nonlinear light generation (2023). **q**, Three-channel active WDM at THz frequencies (2025). **r**, InP nanocavity with extreme dielectric confinement (2024). **s**, Topology-optimized cavity hosting a quantum emitter pair (2024). Panel **a** reprinted from ref. 8, CC BY 4.0. Panel **b** reprinted with permission from ref. 11, Optica Publishing Group. Panel **c** reprinted from ref. 26, CC BY 4.0. Panel **d** reprinted with permission from ref. 29, ACS. Panel **e** reprinted with permission from ref. 36, ACS. Panel **f** reprinted with permission from ref. 39, Optica Publishing Group. Panel **g** reprinted with permission from ref. 2, AIP. Panel **h** reprinted with permission from ref. 45, IEEE. Panel **i** reprinted with permission from ref. 40, SPIE. Panel **j** reprinted from ref. 49, image courtesy of Yi-Kuei Ryan Wu. Panel **k** reprinted with permission from ref. 50, Optica Publishing Group. Panel **l** reprinted from ref. 52, CC BY 4.0. Panel **m** reprinted from ref. 62, CC BY 4.0. Panel **n** reprinted with permission from ref. 72, ACS. Panel **o** reprinted from ref. 76, CC BY 4.0. Panel **p** reprinted from ref. 82, CC BY 4.0. Panel **q** reprinted from ref. 85, CC BY 4.0. Panel **r** reprinted with permission from ref. 94, Optica Publishing Group. Panel **s** reprinted with permission from ref. 116, Optica Publishing Group.

the discrete optimization stage recovered the performance achieved in the continuous stage[2] (Fig. 2g). Several approaches have been proposed to produce manufacturable designs without post-processing. Examples include an always-feasible framework that combines a conditional generator and straight-through gradient estimator to produce designs that are guaranteed to satisfy length-scale constraints,[37] a structure transformation technique that alternates between optimization steps and curvature-constrained structure adjustments to facilitate simpler topologies[45] (Fig. 2h), and the incorporation of a two-level hyperbolic tangent projection function into the optimization process[46]. Another approach seeds density-based topology optimization with a known functional geometry to guide towards ultra-compact, high-performance devices. When applied to a 2D modal multiplexer, 87% of devices conformed to foundry constraints, compared to only 13% of devices designed by conventional topology optimization[47]. A recent open-source software package consolidates previously explored topology optimization techniques with a hybrid time–frequency-domain adjoint-variable formulation, thereby combining the broadband optimization of time-domain solvers with the flexibility and generalizability of frequency-domain solvers. This method achieved broadband performance in large-scale devices, including a 3D polarization splitter and a high-numerical-aperture cylindrical metalens[48]. Departing from topology optimization, a tile-based framework combines direct binary search with fabrication-aware constraints. This method imposes binarization and minimum feature size constraints throughout optimization to avoid post-processing steps such as thresholding[42].

'Fabrication-aware' and robust inverse-design methods embed models of fabrication variability directly into the optimization process. Even DRC-compliant devices may underperform owing to fabrication-induced variability (such as corner rounding, proximity effects, line shortening or sidewall roughness)[43]. Robust inverse design aims to minimize fabrication sensitivity by accounting for fabrication variations throughout the design process[38]. A conventional approach to robustness involves optimizing a structure across an ideal, an over-etched and an under-etched geometry[38,40]. This approach, however, assumes that all three design fields share the same topology, which may not hold for small features. Therefore, actual fabrication outcomes may vary substantially from any of the three geometries[40,43]. By instead calculating the figure of merit based on lithography-predicted geometry, the parameter space can be transformed to be fabrication-aware[43].

Deep-learning models are emerging as a strategy to improve robustness. For example, a deep-learning model was used to predict and compensate for fabrication deviations (Fig. 2i), resulting in significant improvements in predicting fabrication outcomes of complex features relative to uniform bias models[40].

The advancement of robust, fabrication-aware methodologies in academic research has facilitated the translation of inverse design into industry, with an emphasis on compactness and reliability. For example, Google demonstrated a silicon four-channel coarse WDM demultiplexer with consistent performance across 34 chips[49] (Fig. 2j). Industry groups are also leveraging open-source platforms that were developed by academic researchers. Corning used SPINS[2] to design a compact dual-polarization silicon coupler that addresses 14 fibre modes simultaneously[50] (Fig. 2k), whereas Samsung used the FDTD-z platform[3] to design reliable silicon devices to explore the physical limits of photonic components[51].

Given the scaling of inverse-designed device footprint owing to advancements in electromagnetic solvers and the extension of inverse design to commercial foundry processes, some of the first inverse-designed devices have undergone significant enhancements. One exemplary metric for this progress over the past decade is silicon wavelength demultiplexer performance. In Table 1, we present the evolution of inverse-designed WDMs using the first demonstration in 2015 as a baseline. Moreover, scalable foundry-compatible inverse design enables high-performance silicon chips with system-level applications such as optical interconnects. For example, 1.12-Tb s^{-1} natively error-free data transmission was achieved by combining inverse-designed WDMs, mode division multiplexers (MDMs), and surface-normal couplers into a multi-dimensional communication scheme[52] (Fig. 2l).

Inverse design beyond silicon photonics and optical wavelengths

The inverse-design process is material-agnostic and wavelength-agnostic, and parameters and fabrication constraints for any materials and wavelengths can be incorporated into the design process. Consequently, since the initial demonstrations of inverse design in silicon photonics[53–56], III–V materials[57,58] and photovoltaic systems[59,60], inverse design has expanded into diverse material and wavelength systems, providing unique functionalities. Here, we describe recent progress on inverse design in now-mainstream photonic materials:

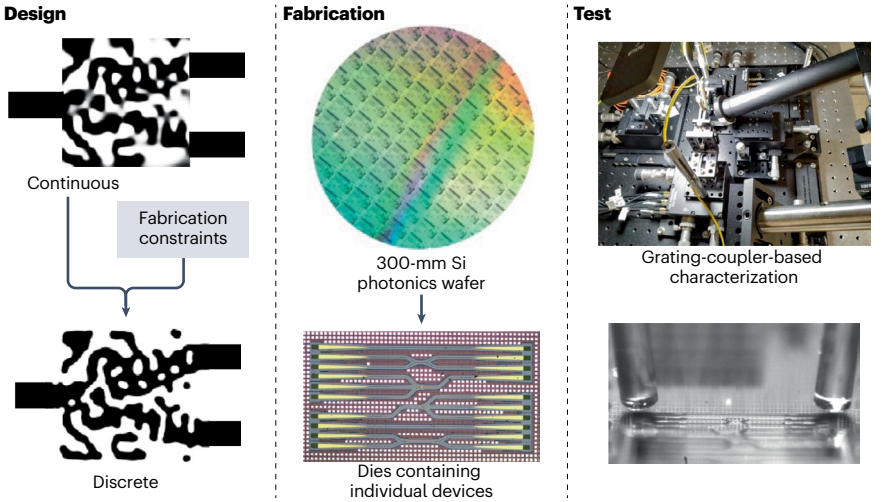

Fig. 3 | Inverse-design workflow for commercial silicon photonics foundries. During the design phase, fabrication constraints are applied to obtain the discrete design. The final device design is then used to produce the mask pattern. During fabrication, dies containing individual devices are produced from 300 mm Si wafers. The devices are then tested, in this example, in a vertical transmission measurement set-up. Reprinted with permission from ref. 36, ACS.

silicon nitride and lithium niobate, as well as the leading quantum photonic materials diamond and silicon carbide. In this section, we focus on linear inverse design, whereas in the next section, we describe direct nonlinear inverse design in these materials. Moreover, we also describe recent progress on utilizing inverse design in terahertz and microwave wavelength ranges.

Silicon nitride and lithium niobate

Silicon nitride has emerged as a promising material in integrated photonics, as it features ultra-low material loss[61] that provides order loss (dB m^{-1}) at telecommunication and visible wavelengths, and provides favourable nonlinear optical properties based on its third-order ($\chi^{(3)}$) nonlinearities.

Similar to silicon photonics, as described in the previous section, inverse design was used to achieve silicon nitride photonic blocks with better performance and compact footprints: WDMs and MDMs[62,63] (Fig. 2m), power splitters[64,65] and polarization beam splitters[62,66]. Shrinking footprint is a grand challenge here because of the low index contrast between silicon nitride and the cladding, which requires a larger device footprint than in typical silicon photonics systems[67]. For instance, inverse-designed WDMs can achieve low insertion loss and crosstalk with a moderate minimum feature size of 160 nm and only a 24 μm × 24 μm device size, which is significantly smaller than traditional Mach–Zehnder interferometers or ring resonator-based components[67,68].

In the past decade, thin-film lithium niobate has also emerged as a photonics platform that provides low propagation loss and large $\chi^{(2)}$ and $\chi^{(3)}$ nonlinearity in a broad wavelength range, from visible to terahertz wavelengths. However, similar to silicon nitride, lithium niobate has a low refractive index, making the design problem challenging. Moreover, lithium niobate fabrication poses unique challenges, such as sloped sidewalls, and the lithium niobate birefringence further complicates the design process. Recently, inverse-design techniques incorporating both birefringence and sidewall features have been demonstrated. A fabrication-aware framework tailored to lithium niobate on insulator platforms was proposed, involving a slope-processing algorithm that decomposes sloped sidewalls into discrete layers[69].

One exemplary challenge in thin-film lithium niobate is the realization of a grating coupler because of the low index contrast between lithium niobate and the cladding layer. High-efficiency inverse-designed grating couplers with 3.18 dB and 1.97 dB of coupling efficiency were demonstrated in refs. 70,71. Both studies incorporate the sidewall angle of lithium niobate into the simulation model used in optimization, and hence the resulting simulated efficiency is closer to the actual value. However, these studies mostly optimize a small set of discrete parameters that describe the shape of gratings (namely, widths and gaps of gratings) and do not really conduct a full-scale optimization. A more general inverse-design technique for lithium niobate was proposed based on topology optimization[72]. This strategy is similar to topology optimization-based inverse-design approaches in conventional silicon photonics, consisting of an optimization step with a continuous permittivity distribution, optimization with binarization and discrete optimization that enforces a minimum feature size requirement. After the discrete optimization step, additional optimization steps add a sidewall projection model into the simulation model to get a final design with full consideration of sidewall features. The resulting mode multiplexer (Fig. 2n), waveguide crossing and waveguide bend demonstrated small insertion loss and crosstalk and significant footprint reduction compared to conventional designs. This study was performed on *z*-cut lithium niobate, which is convenient for inverse design in a transverse electric mode configuration. However, thin-film lithium niobate devices utilizing $\chi^{(2)}$ or the Pockels effect (r_{33}) use *x*-cut lithium niobate, which requires birefringence consideration in the optimization step.

Recently, an improved topology optimization method with both sidewall and birefringence considerations was proposed[73], which led to a Y-splitter design in *x*-cut lithium niobate with 0.70-dB insertion loss. Aside from the typical component designs for compact, high-performance thin-film lithium niobate photonic design, inverse design is being utilized in various functions such as mode converters for second-harmonic generation, spontaneous parametric down-conversion[74], and on-chip mirrors for enhanced optical gain in erbium-doped lithium niobate waveguides[75].

Quantum photonic materials

Performance requirements are even more stringent in the quantum regime than in classical photonics, as loss of even individual photons has dramatic consequences on the system performance. Often,

quantum photonic devices operate in extreme conditions, such as low temperature and high vacuum, thereby requiring new ways of probing the systems. Inverse design has an essential role in finding new, more suitable geometries. Moreover, many suitable quantum materials (such as diamond) have even more stringent fabrication constraints than silicon nitride or lithium niobate.

Direct patterning of inverse-designed coupler structures has been adopted as an efficient and simple way of light coupling for such quantum systems. For example, efficient inverse-designed power splitters and vertical couplers providing 25% coupling efficiency with 1 μm × 1 μm footprint in diamond were demonstrated and were compatible with stringent diamond fabrication[76] (Fig. 2o). Heterogeneous structures comprising bulk diamond hosting a nitrogen vacancy colour centre and an inverse-designed gallium phosphide (GaP) pattern on top were also demonstrated[77], showing a 14-fold enhancement of zero phonon line emission from the nitrogen vacancy centre, which was placed 100 nm below the surface. Another example is hexagonal boron nitride (hBN), which is frequently used as an insulating capping layer or itself as a host of quantum emitters. Inverse design provides a huge advantage in footprint, which is crucial in 2D materials such as hBN owing to the small size of flakes. A monolithic hBN inverse-designed grating coupler with 35% outcoupling efficiency from single-photon emitters in hBN was demonstrated[78], as well as more advanced nanophotonic components on hBN encapsulating $MoSe_2$ (ref. 79), including a compact grating coupler with 11% efficiency, waveguide mirrors with 99.5% reflectance, and metasurfaces that increased the collection efficiency of dark excitons.

Silicon carbide is yet another example of an emerging quantum material, and inverse design has been used to design grating couplers in 4H-silicon carbide for first harmonic (1,555 nm) and second harmonic (777.5 nm), enabling a second-order frequency conversion in microring resonators[80]. Additionally, Kerr-nonlinearity-mediated optical parametric oscillators and frequency combs in 4H-silicon carbide on insulator systems have been demonstrated, with inverse-designed vertical couplers with 31% peak efficiency and broad bandwidth (1,450–1,600 nm)[81]. Direct inverse design of cavities was also adopted for quantum frequency combs[82], wherein an inverse-designed Fabry–Perot cavity was used to create frequency combs in C-band and visible wavelengths through the $\chi^{(2)}$ and $\chi^{(3)}$ of silicon carbide (Fig. 2p).

Fundamentally, any system that is described by Maxwell's equations can benefit from an inverse-design tool similar to those used for visible and telecommunication wavelength regimes as previously described. Terahertz integrated photonics[83,84] is an emerging field wherein photonics-based devices can process terahertz signals, providing much more compact and versatile designs than those based on microwave engineering. A three-channel WDM operating at the 2–3-THz range, creating three terahertz emission antennas with different frequency ranges split from a shared co-integrated quantum cascade laser (QCL) source, was recently demonstrated[85] (Fig. 2q). The same inverse-design tool that is used for inverse design at telecommunication wavelengths[2] is utilized for this terahertz work, which shows a universality of inverse-design methodology. Additionally, the same team demonstrated a low-reflectivity end facet of the metallic waveguide used in the QCL device[86] and enhanced the slope efficiency (slope between power and injected current) by seven times.

For free-space terahertz photonic elements, inverse design has been used to design an electromagnetically induced transparency (EIT) in a metasurface structure comprising germanium on quartz and a patterned gold layer on top[87]. This metasurface can modulate the EIT based on the visible light pumping into the germanium film, controlling its conductivity owing to the carrier excitation. Inverse design has been used in electromagnetic systems with wavelengths longer than terahertz, namely, microwave and magnonic systems, to produce high-performance, versatile devices. S-Matrix engineering has enabled parallel computing[88], filter and divider design[89], and a dual-polarization surface launcher for a dielectric waveguide[90], demonstrating complex functionalities that could not be implemented in traditional microwave engineering. In magnonic systems, the propagation of spin waves in magnetic materials such as yttrium iron garnet (YIG) can be manipulated by putting nano-patterns or applying an external magnetic field. The general idea of inverse design in a magnonic device was demonstrated in a device consisting of a 10 × 10 array of 100 nm × 100 nm YIG patches (represented by 10 × 10 array of magnetization)[91]. These patches can be inverse-designed for frequency multiplexing and as circulators with fixed external fields and a nonlinear switch that can be reconfigured by changing the external magnetic fields. A reconfigurable magnonic device that can tune the response based on an array, with 49 current sources, placed on a YIG film was recently developed[92], providing a general scheme for reconfigurable magnonic devices with target transmission functionality.

Nonlinear inverse design

Optical cavities (resonators) are the workhorses of laser physics, nonlinear optics and quantum optics (cavity quantum electrodynamic (QED)). The goal in laser design, optimization of nonlinear processes, or design of cavity QED systems is increasing the cavity quality factor Q while reducing mode volume V. This leads to a reduction of the lasing threshold and improved efficiency, as well as a reduction of the threshold for nonlinear local processes, and the crossing into the strong-coupling regime of cavity QED.

Since the early work on direct inverse design of photonic cavities to maximize Q/V (ref. 93), more efforts have been undertaken in this direction[94–97]. These include inverse design of nanoscale optical resonators in photonic material platforms with dipoles approximating

Table 1 | Progress in inverse-design silicon wavelength demultiplexer performance

Year	Channel spacing (nm)	Insertion loss (dB)	Crosstalk (dB)	No. of channels	Inverse-design footprint	Total footprint (μm^2)	Fabrication process	Ref.
2015	250	1.8–2.4	−11	2	2.8 μm × 2.8 μm = 7.84 μm^2	7.84	University	53
2018	40	2.29–2.82	−10.7	3	5.5 μm × 4.5 μm = 24.75 μm^2	24.75	University	54
2024	20	2–3.3	−19 to −26	4	14 μm × 16 μm = 224 μm^2	224	Commercial foundry	49
2025	15	1.86–3.9	−41	2	12 μm × 12 μm = 144 μm^2	279[a]	University	127

[a]This device uses Bragg filters that are not included in the optimization region and add to total device area.

quantum emitters[98]. Such optimized photonic cavities for Q/V maximization have been experimentally demonstrated[94] (Fig. 2r). Aside from maximizing Q/V, inverse-designed cavities implementing diverse laser polarizations and beam shapes[99] have also been demonstrated.

Likewise, a majority of nonlinear photonic circuits utilize high-Q resonators to get resonance-enhanced nonlinear effects. However, such nonlinear effects are heavily affected by the dispersion of the resonators. Unlike traditional dispersion-engineering methods, which mostly optimize waveguide cross-sectional geometry[100], inverse design enables more robust and versatile dispersion engineering[101]. Prior work on inverse design of nonlinear optical systems has focused on the inverse design of coupled linear problems[82], but in more recent efforts, nonlinear equations are directly optimized to achieve target performance.

In the application of Kerr-comb generation, two complementary efforts illustrate this approach. First, 'meta-dispersion' treats mode-by-mode frequency splitting as a programmable degree of freedom, letting designers match user-specified comb spectra and flatten bands via controlled multimode hybridization, effectively inverting the Lugiato–Lefever dynamics to a spectral target[102]. In a first work[103], the researchers used a genetic algorithm to optimize the parameters of concentric microresonators in conjunction with a Lugiato–Lefever equation solver based on a deep neural network to enhance the flatness of soliton combs in silicon nitride. Similarly, in another work[102], the shape of a Ta_2O_5 photonic crystal ring resonator was optimized by creating a meta-dispersion that enables target comb shapes such as flat-top or Gaussian-shape combs.

An alternative approach for the dispersion engineering of microresonators is inserting an inverse-designed component in a resonator with a tailored phase response. In silicon photonics, such functionality was experimentally demonstrated[101] by placing a reflective element with target frequency-dependent reflection phase in a microresonator. Recent demonstrations of inverse-designed reflectors in silicon nitride[63,104] have successfully exhibited high reflectivity (97– 98%) in a broad optical wavelength range, which is promising for realizing high-Q on-chip Fabry–Perot resonators with dispersion engineering. Another approach is inverse designing a mode converter between different mode families to design a target mode-crossing[105]. Finally, comb initiation and stabilization can be cast as an optimization problem over pump parameters. Towards this goal, genetic algorithms have been used to discover operating points for stable, target-shaped combs[106].

Alongside Q factor and dispersion engineering in nonlinear integrated photonics, inverse design has been used to directly optimize nonlinear interactions. Phase-matching for four-wave mixing was incorporated as the loss function for a silicon-on-insulator grating cavity at telecom wavelengths, yielding a compact structure with high-Q resonances at target wavelengths, and enhancing pair-generation rate and coincidence-to-accidental ratio[107]. Inverse design has also been applied to nonlinear metasurfaces, particularly those based on multiple quantum wells (MQWs)[108]. MQWs supporting intersubband transitions (ISTs) exhibit giant nonlinearities that can be engineered via heterostructure thickness optimization at the fundamental and harmonic wavelengths. Combined with resonator geometry optimization to excite Mie modes that enhance pump coupling to the IST and local field enhancement, large second-harmonic generation (SHG) efficiencies have been demonstrated[109]. Recently, a topology-optimized MQW metasurface based on the optimization of an IST heterostructure and far-field directionality with fabrication constraint consideration was experimentally demonstrated with a record SHG efficiency of 0.38 mW W^{-2} (ref. 110). For plasmonic platforms, a TiO_2–Al_2O_3–HfO_2 nanolaminate with broken z-symmetry was combined with deep-learning-based inverse-designed metallic structures, yielding an enhanced SHG response at 840-nm excitation[111].

Similar to photonic inverse design, inverse design of quantum systems implies posing a quantum objective (for example, a target steady-state entangled density matrix) and optimizing the electromagnetic environment, or driving the quantum system so that this target state is achieved (Fig. 4). Beyond linear photonics optimization in quantum materials, as described in the previous section, or optimization of resonators or multi-port interferometer[112] for quantum optics experiments, efforts have also focused on the space of quantum control and generalized Floquet driving. This line of 'quantum optimization' was initially pursued using gradient-based ascent methods, in which the objective function is defined by specific metrics of the quantum systems[113]. Recently, these methods led to utilizing a more robust numerical optimization landscape. For example, adjoint optimization has been used to find an optimal drive for a quantum system, which leads to superradiant effects or improved quantum transduction efficiency in inhomogeneously broadened ensembles[114,115].

Recent efforts on topology-optimized cavities have moved beyond quantum control problems: under continuous-wave drive and using moderate-index dielectrics, the design explicitly maximizes dissipative coupling and prepares high-fidelity Bell and W states of spatially separated emitters, linking photonic structure directly to open-system steady states[116] (Fig. 2s). In parallel, topological waveguide-QED theory clarifies which bath properties are worth targeting: band gaps, edge modes and nontrivial winding can host chiral bound states that mediate long-range, tunable interactions, and topology-dependent sub-radiance or superradiance[117]. For quantum light sources, multi-objective formulations that jointly maximize Purcell factor and collection efficiency already point towards end-to-end objectives (brightness, indistinguishability) under realistic geometry and fabrication constraints[118]. A practical recipe follows: encode fidelity or source metrics in the objective, co-optimize coherent and/or dissipative couplings by shaping the local density of states, and include tolerances, spectral diffusion and bandwidth terms so designs transfer cleanly to a variety of suitable quantum materials with reproducible, high-fidelity performance.

Conclusion

The field of photonic inverse design has been advancing rapidly over the past decade, moving beyond proof-of-concept demonstrations relying on university fabrication facilities. The use of inverse design in photonics is certainly not only an academic curiosity anymore, but it is also getting a broad acceptance beyond academia, in which it is actively used to address problems wherein traditional photonics fails (such as higher-efficiency, broadband couplers for optical interconnects made in commercial foundries)[119]. Major progress has been made in translating inverse design to commercial silicon foundries and in developing new electromagnetic solvers and tools capable of addressing larger design footprints, even full metasurface design. Being materials-agnostic and wavelength-agnostic, inverse design has naturally moved into materials beyond silicon and wavelengths outside of the optical band. Recognizing the success of photonics inverse design, similar approaches are emerging in the design of scalable nonlinear and quantum systems, in the context of dispersion engineering, in

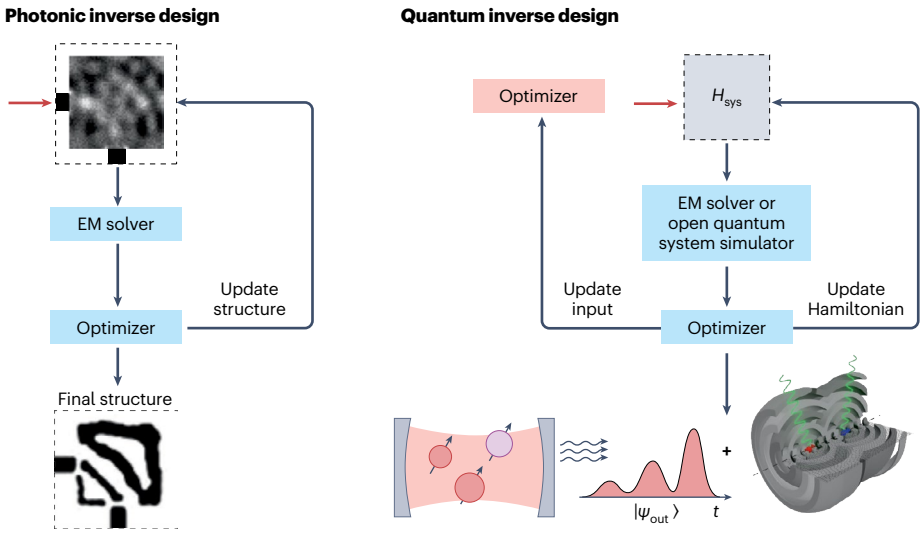

Fig. 4 | Quantum inverse design. Analogous to photonic inverse design (left), a similar approach can be applied to designing quantum systems (right). The parameters of the system (dielectric constant distribution, global electric field, optical drive modulation and so on) are optimized to achieve the desired system Hamiltonian (H_{sys}). In addition to electromagnetic (EM) solvers, solvers such as open quantum system simulators can be used in the inverse-design loop. Left schematic reprinted with permission from ref. 114, ACS. Right schematic reprinted with permission from ref. 116, Optica Publishing Group.

quantum control and in the design of environments to achieve target Hamiltonians.

Looking forward, we will certainly see even more inverse-design applications in other research areas and fields, as this approach has proven itself as a tool to solve difficult problems wherein human intuition and standard building blocks fail. In fact, big initiatives are already emerging in academia, in government and in industry focused on the use of artificial-intelligence tools in scientific discovery and to accelerate engineering, such as the discovery of new materials and chip design, or to advance quantum information hardware[120–122]. In large-scale photonics inverse design, we anticipate that artificial-intelligence tools may be helpful for structure initialization or defining the objective function, which are now still dependent on the experienced researcher. Further advancement of computing bounds (in particular, making them stricter) will eventually help to choose initial device footprint for a specific problem instead of going through trial and error[123–126]. Moreover, with further artificial intelligence hardware advancements, we expect that even more powerful electromagnetic simulators and inverse-design tools will emerge[3,5], capable of solving larger device footprints or possibly designing full systems.

Although inverse design has already proven itself as a tool that can greatly enhance research and engineering capabilities, it will not be a replacement for skilled researchers and their creativity. It is important to remember that although these tools seem very powerful on the outside, they are not intelligent or creative; instead, they are only performing complex computational tasks very fast — the tasks that we as researchers programmed them and assigned them to do. In the case of photonics, these are essentially solvers of Maxwell's equations combined with adjoint optimization and backpropagation techniques, allowing fast calculation of gradients and gradient descent. Without human ingenuity, critical thinking and guidance in defining problems and bringing up new ideas, even the best computing hardware and software will not be capable of making real breakthroughs in science and advancing knowledge. Therefore, the availability of these powerful tools should not be the reason to stop teaching students underlying subjects such as electromagnetism or photonics. On the contrary, the success of inverse design should be the motivation to strengthen education and training across subjects (such as electromagnetics + computer science), as this is an example of how creative researchers who are well-trained in multiple fields can greatly advance science and engineering.

Published online: 20 April 2026

References

1. Molesky, S. et al. Inverse design in nanophotonics. *Nat. Photon.* **12**, 659–670 (2018).
2. Su, L. et al. Nanophotonic inverse design with SPINS: software architecture and practical considerations. *Appl. Phys. Rev.* **7**, 011407 (2020).
3. Lu, J. et al. Overcoming memory bandwidth limitations In GPU-accelerated finite-difference time-domain simulation: a systolic update scheme. *IEEE Antennas Propag. Mag.* https://doi.org/10.1109/MAP.2026.3668263 (2026).
4. Oskooi, A. F. et al. Meep: a flexible free-software package for electromagnetic simulations by the FDTD method. *Comput. Phys. Commun.* **181**, 687–702 (2010).
5. Mahlau, Y. et al. FDTDX: high-performance open-source FDTD simulation with automatic differentiation. *J. Open Source Softw.* **11**, 8912 (2026).
6. Li, Z., Pestourie, R., Lin, Z., Johnson, S. G. & Capasso, F. Empowering metasurfaces with inverse design: principles and applications. *ACS Photon.* **9**, 2178–2192 (2022).
7. Ji, W. et al. Recent advances in metasurface design and quantum optics applications with machine learning, physics-informed neural networks, and topology optimization methods. *Light Sci. Appl.* **12**, 169 (2023).
8. Li, Z. et al. Inverse design enables large-scale high-performance meta-optics reshaping virtual reality. *Nat. Commun.* **13**, 2409 (2022).
9. So, S. et al. Multicolor and 3D holography generated by inverse-designed single-cell metasurfaces. *Adv. Mater.* **35**, 2208520 (2023).
10. Backer, A. S. Computational inverse design for cascaded systems of metasurface optics. *Opt. Express* **27**, 30308 (2019).
11. Lin, Z. et al. End-to-end metasurface inverse design for single-shot multi-channel imaging. *Opt. Express* **30**, 28358–28370 (2022).
12. Harper, E. S., Coyle, E. J., Vernon, J. P. & Mills, M. S. Inverse design of broadband highly reflective metasurfaces using neural networks. *Phys. Rev. B* **101**, 195104 (2020).
13. Lin, R., Zhai, Y., Xiong, C. & Li, X. Inverse design of plasmonic metasurfaces by convolutional neural network. *Opt. Lett.* **45**, 1362–1365 (2020).
14. Cai, H. et al. Inverse design of metasurfaces with non-local interactions. *npj Comput. Mater.* **6**, 116 (2020).
15. Zhou, M. et al. Inverse design of metasurfaces based on coupled-mode theory and adjoint optimization. *ACS Photon.* **8**, 2265–2273 (2021).
16. Xu, Y. et al. Physics-informed inverse design of programmable metasurfaces. *Adv. Sci.* **11**, 2406878 (2024).
17. Jiang, J. & Fan, J. A. Simulator-based training of generative neural networks for the inverse design of metasurfaces. *Nanophotonics* **9**, 1059–1069 (2020).
18. Zhu, R. et al. Phase-to-pattern inverse design paradigm for fast realization of functional metasurfaces via transfer learning. *Nat. Commun.* **12**, 2974 (2021).
19. Tanriover, I., Lee, D., Chen, W. & Aydin, K. Deep generative modeling and inverse design of manufacturable free-form dielectric metasurfaces. *ACS Photon.* **10**, 875–883 (2023).

20. Mall, A., Patil, A., Sethi, A. & Kumar, A. A cyclical deep learning based framework for simultaneous inverse and forward design of nanophotonic metasurfaces. *Sci. Rep.* **10**, 19427 (2020).
21. Liu, Z., Zhu, D., Rodrigues, S. P., Lee, K.-T. & Cai, W. Generative model for the inverse design of metasurfaces. *Nano Lett.* **18**, 6570–6576 (2018).
22. Cordaro, A. et al. Solving integral equations in free space with inverse-designed ultrathin optical metagratings. *Nat. Nanotechnol.* **18**, 365–372 (2023).
23. Dainese, P. et al. Shape optimization for high efficiency metasurfaces: theory and implementation. *Light Sci. Appl.* **13**, 300 (2024).
24. Zhelyeznyakov, M. et al. Large area optimization of meta-lens via data-free machine learning. *Commun. Eng.* **2**, 60 (2023).
25. Skarda, J. et al. Low-overhead distribution strategy for simulation and optimization of large-area metasurfaces. *npj Comput. Mater.* **8**, 78 (2022).
26. Roberts, G. et al. 3D-patterned inverse-designed mid-infrared metaoptics. *Nat. Commun.* **14**, 2768 (2023).
27. Chen, M., Chan, K. F., Hammond, A. M., Chan, C.-H. & Johnson, S. G. Inverse design o f 3D-printable metalenses with complementary dispersion for terahertz imaging. *ACS Photon.* **12**, 3510–3516 (2025).
28. Munley, C. et al. Inverse-designed meta-optics with spectral-spatial engineered response to mimic color perception. *Adv. Opt. Mater.* **10**, 2200734 (2022).
29. Sun, M. et al. Scalable freeform optimization of wide-aperture 3D metalenses by zoned discrete axisymmetry. *ACS Photon.* **12**, 3163–3171 (2025).
30. Strauch, A., Augenstein, Y. & Rockstuhl, C. Inverse design of 3D-printed photonic wire bond couplers — benchmarking different optimization strategies. *J. Light. Technol.* **43**, 6797–6806 (2025).
31. Di Domenico, G., Weisman, D., Panichella, A., Roitman, D. & Arie, A. Large-scale inverse design of a planar on-chip mode sorter. *ACS Photon.* **9**, 378–382 (2022).
32. Sapra, N. V. et al. Inverse design and demonstration of broadband grating couplers. *IEEE J. Sel. Top. Quantum Electron.* **25**, 1–7 (2019).
33. Pita, J., Dainese, P. & Ménard, M. Inverse design fiber-to-chip couplers for the O- and C-bands. *Opt. Lett.* **50**, 1973–1976 (2025).
34. Hammond, A. M., Slaby, J. B., Probst, M. J. & Ralph, S. E. Multi-layer inverse design of vertical grating couplers for high-density, commercial foundry interconnects. *Opt. Express* **30**, 31058–31072 (2022).
35. Huang, S.-Y. & Barz, S. Compact inverse designed vertical coupler with bottom reflector for sub-decibel fiber-to-chip coupling on silicon on insulator platform. *Sci. Rep.* **15**, 2925 (2025).
36. Piggott, A. Y. et al. Inverse-designed photonics for semiconductor foundries. *ACS Photon.* **7**, 569–575 (2020).
37. Schubert, M. F., Cheung, A. K. C., Williamson, I. A. D., Spyra, A. & Alexander, D. H. Inverse design of photonic devices with strict foundry fabrication constraints. *ACS Photon.* **9**, 2327–2336 (2022).
38. Hammond, A. M., Oskooi, A., Johnson, S. G. & Ralph, S. E. Photonic topology optimization with semiconductor-foundry design-rule constraints. *Opt. Express* **29**, 23916–23938 (2021).
39. Zhang, G., Xu, D.-X., Grinberg, Y. & Liboiron-Ladouceur, O. Experimental demonstration of robust nanophotonic devices optimized by topological inverse design with energy constraint. *Photon. Res.* **10**, 1787–1802 (2022).
40. Grinberg, Y. et al. Inverse design of robust photonic components. In *Proc. SPIE Integr. Opt.* Vol. 12424 (eds García-Blanco, S. M. & Cheben, P.) 124240C (SPIE, 2023).
41. Sideris, C., Khachaturian, A., White, A. D., Bruno, O. P. & Hajimiri, A. Foundry-fabricated grating coupler demultiplexer inverse-designed via fast integral methods. *Commun. Phys.* **5**, 68 (2022).
42. Yu, I. et al. Structured inverse design: a tile-based approach for practical photonic integration. In *Proc. SPIE Opt. Des. Autom.* Vol. 13601 (eds Heinz-Garcia, J. & Gregory, G.) 145–157 (SPIE, 2025).
43. Raza, S., Hammood, M., Jaeger, N. A. F. & Chrostowski, L. Fabrication-aware inverse design for shape optimization photonic integrated circuits. *Opt. Lett.***50**, 117–120 (2025).
44. Zhang, G., Xu, D.-X., Grinberg, Y. & Liboiron-Ladouceur, O. Topological inverse design of nanophotonic devices with energy constraint. *Opt. Express* **29**, 12681–12695 (2021).
45. Chen, Y. et al. Inverse design of free-form devices with fabrication-friendly topologies based on structure transformation. *J. Light Technol.* **41**, 4762–4776 (2023).
46. Liang, H. et al. Topological inverse design of fabrication-constrained nanophotonic devices via an adaptive projection method. *Opt. Lett.* **47**, 5401–5404 (2022).
47. Hiesener, J. M., Kaylor, C. A., Wong, J. J., Agarwal, P. & Ralph, S. E. Seeded topology optimization for commercial foundry integrated photonics. *APL Photon.* **10**, 096101 (2025).
48. Hammond, A. M. et al. High-performance hybrid time/frequency-domain topology optimization for large-scale photonics inverse design. *Opt. Express* **30**, 4467–4491 (2022).
49. Cheung, A. K. C. et al. Inverse-designed CWDM demultiplexer operated in O-band. In *Opt. Fiber Commun. Conf. Exhibit.* (Optica, 2024).
50. Ruiz, J. L. P. et al. Compact dual-polarization silicon integrated couplers for multicore fibers. *Opt. Lett.* **46**, 3649–3652 (2021).
51. Sofronov, A., Yakovleva, D. & Yakubovich, A. Accelerated inverse design of passive Si photonics. Preprint at https://doi.org/10.48550/arXiv.2505.03352 (2025).
52. Yang, K. Y. et al. Multi-dimensional data transmission using inverse-designed silicon photonics and microcombs. *Nat. Commun.* **13**, 7862 (2022).
53. Piggott, A. Y. et al. Inverse design and demonstration of a compact and broadband on-chip wavelength demultiplexer. *Nat. Photon.* **9**, 374–377 (2015).
54. Su, L., Piggott, A. Y., Sapra, N. V., Petykiewicz, J. & Vučković, J. Inverse design and demonstration of a compact on-chip narrowband three-channel wavelength demultiplexer. *ACS Photon.* **5**, 301–305 (2018).
55. Lalau-Keraly, C. M., Bhargava, S., Miller, O. D. & Yablonovitch, E. Adjoint shape optimization applied to electromagnetic design. *Opt. Express* **21**, 21693–21701 (2013).
56. Michaels, A. & Yablonovitch, E. Inverse design of near unity efficiency perfectly vertical grating couplers. *Opt. Express* **26**, 4766–4779 (2018).
57. Sitawarin, C., Jin, W., Lin, Z. & Rodriguez, A. W. Inverse-designed photonic fibers and metasurfaces for nonlinear frequency conversion [Invited]. *Photon. Res.* **6**, B82–B89 (2018).
58. Lin, Z., Lončar, M. & Rodriguez, A. W. Topology optimization of multi-track ring resonators and 2D microcavities for nonlinear frequency conversion. *Opt. Lett.* **42**, 2818–2821 (2017).
59. Ganapati, V., Miller, O. D. & Yablonovitch, E. Light trapping textures designed by electromagnetic optimization for subwavelength thick solar cells. *IEEE J. Photovolt.* **4**, 175–182 (2014).
60. Xiao, T. P. et al. Diffractive spectral-splitting optical element designed by adjoint-based electromagnetic optimization and fabricated by femtosecond 3D direct laser writing. *ACS Photon.* **3**, 886–894 (2016).
61. Xiang, C., Jin, W. & Bowers, J. E. Silicon nitride passive and active photonic integrated circuits: trends and prospects. *Photon. Res.* **10**, A82–A96 (2022).
62. Pita Ruiz, J. L., Dalvand, N. & Ménard, M. Integrated silicon nitride devices via inverse design. *Nat. Commun.* **16**, 9307 (2025).
63. Bi, T. et al. Inverse-designed silicon nitride nanophotonics. Preprint at https://doi.org/10.48550/arXiv.2505.13383 (2025).
64. Song, C. et al. Ultracompact and broadband Si_3N_4 Y-branch splitter using an inverse design method. *Opt. Express* **32**, 46080–46089 (2024).
65. Slaby, J. B., Hammond, A. M. & Ralph, S. E. Compact inverse designed integrated 1×3 silicon nitride balanced optical power splitter. In *IEEE Photon. Conf.* (IEEE, 2022).
66. Cong, Y. et al. Inverse design of an ultra-compact polarization beam splitter. *Appl. Opt.* **64**, 1288–1294 (2025).
67. Yang, Y.-D., Li, Y., Huang, Y.-Z. & Poon, A. W. Silicon nitride three-mode division multiplexing and wavelength-division multiplexing using asymmetrical directional couplers and microring resonators. *Opt. Express* **22**, 22172–22183 (2014).
68. Gao, G. et al. Silicon nitride O-band (de)multiplexers with low thermal sensitivity. *Opt. Express* **25**, 12260–12267 (2017).
69. Qiao, Y., Qiu, C., Chen, Y., Qin, L. & Wang, L. A fabrication-aware inverse design method for thin-film lithium niobate photonic devices. *Opt. Commun.* **596**, 132506 (2025).
70. Xue, C. et al. Inverse design and fabrication of high-efficiency perfectly vertical LNOI grating couplers. *Opt. Lett.* **50**, 864–867 (2025).
71. Zhan, B., Zhang, H. & Liu, X. Inverse design of high-efficiency lithium-niobate-on-insulator grating couplers with user-defined apodization. *Opt. Express* **33**, 11221–11230 (2025).
72. Shang, C. et al. Inverse-designed lithium niobate nanophotonics. *ACS Photon.* **10**, 1019–1026 (2023).
73. Lyu, J. et al. Inverse-designed 1×2 power splitter on X-cut thin-film lithium niobate platform by DUV photonic integration. *Opt. Express* **33**, 34727–34735 (2025).
74. Kwon, K. et al. Photon-pair generation using inverse-designed thin-film lithium niobate mode converters. *APL Photon.* **9**, 056108 (2024).
75. Wei, Z. et al. Erbium-doped lithium niobate waveguide amplifier enhanced by an inverse-designed on-chip reflector. *Opt. Lett.* **50**, 3624–3627 (2025).
76. Dory, C. et al. Inverse-designed diamond photonics. *Nat. Commun.* **10**, 3309 (2019).
77. Chakravarthi, S. et al. Inverse-designed photon extractors for optically addressable defect qubits. *Optica* **7**, 1805–1811 (2020).
78. Li, C. et al. Integration of hBN quantum emitters in monolithically fabricated waveguides. *ACS Photon.* **8**, 2966–2972 (2021).
79. Gelly, R. J. et al. An inverse-designed nanophotonic interface for excitons in atomically thin materials. *Nano Lett.* **23**, 8779–8786 (2023).
80. Lukin, D. M. et al. 4H-Silicon-carbide-on-insulator for integrated quantum and nonlinear photonics. *Nat. Photon.* **14**, 330–334 (2020).
81. Guidry, M. A. et al. Optical parametric oscillation in silicon carbide nanophotonics. *Optica* **7**, 1139–1142 (2020).
82. Yang, J., Guidry, M. A., Lukin, D. M., Yang, K. & Vučković, J. Inverse-designed silicon carbide quantum and nonlinear photonics. *Light Sci. Appl.* **12**, 201 (2023).
83. Sengupta, K., Nagatsuma, T. & Mittleman, D. M. Terahertz integrated electronic and hybrid electronic–photonic systems. *Nat. Electron.* **1**, 622–635 (2018).
84. Rajabali, S. & Benea-Chelmus, I.-C. Present and future of terahertz integrated photonic devices. *APL Photon.* **8**, 080901 (2023).
85. Digiorgio, V. et al. On-chip, inverse-designed active wavelength division multiplexer at THz frequencies. *Nat. Commun.* **16**, 7711 (2025).
86. Senica, U. et al. Broadband surface-emitting THz laser frequency combs with inverse-designed integrated reflectors. *APL Photon.* **8**, 096101 (2023).
87. He, W. et al. Ultrafast all-optical terahertz modulation based on an inverse-designed metasurface. *Photon. Res.* **9**, 1099–1108 (2021).
88. Camacho, M., Edwards, B. & Engheta, N. A single inverse-designed photonic structure that performs parallel computing. *Nat. Commun.* **12**, 1466 (2021).
89. Karahan, E. A. et al. Deep-learning enabled generalized inverse design of multi-port radio-frequency and sub-terahertz passives and integrated circuits. *Nat. Commun.* **15**, 10734 (2024).

90. Huang, J.-Y., Molisch, A. F. & Sideris, C. Concurrent dual polarization dielectric waveguide interconnect using inverse designed dual-mode surface antenna launcher. In *IEEE Int. Symp. Antennas Propag. USNC-URSI Radio Sci. Meet. (USNC-URSI)* 1769–1770 (IEEE, 2023).
91. Wang, Q., Chumak, A. V. & Pirro, P. Inverse-design magnonic devices. *Nat. Commun.* **12**, 2636 (2021).
92. Zenbaa, N. et al. A universal inverse-design magnonic device. *Nat. Electron.* **8**, 106–115 (2025).
93. Lu, J., Boyd, S. & Vučković, J. Inverse design of a three-dimensional nanophotonic resonator. *Opt. Express* **19**, 10563–10570 (2011).
94. Xiong, M. et al. Experimental realization of deep sub-wavelength confinement of light in a topology-optimized InP nanocavity. *Opt. Mater. Express* **14**, 397–406 (2024).
95. Wang, F., Christiansen, R. E., Yu, Y., Mørk, J. & Sigmund, O. Maximizing the quality factor to mode volume ratio for ultra-small photonic crystal cavities. *Appl. Phys. Lett.* **113**, 241101 (2018).
96. Mørk, J. et al. Nanostructured semiconductor lasers. *IEEE J. Sel. Top. Quantum Electron.* **31**, 1–17 (2025).
97. Jokisch, B. M. et al. Efficient first-principles inverse design of nanolasers. *Laser Photonics Rev.* https://doi.org/10.1002/lpor.202501614 (2026).
98. Martinez de Aguirre Jokisch, B. et al. Omnidirectional gradient force optical trapping in dielectric nanocavities by inverse design. *ACS Photon.* **11**, 5118–5127 (2024).
99. Diez, I., Krysa, A. & Luxmoore, I. J. Inverse design of whispering-gallery nanolasers with tailored beam shape and polarization. *ACS Photon.* **10**, 968–976 (2023).
100. Okawachi, Y. et al. Bandwidth shaping of microresonator-based frequency combs via dispersion engineering. *Opt. Lett.* **39**, 3535–3538 (2014).
101. Ahn, G. H. et al. Photonic inverse design of on-chip microresonators. *ACS Photon.* **9**, 1875–1881 (2022).
102. Lucas, E., Yu, S.-P., Briles, T. C., Carlson, D. R. & Papp, S. B. Tailoring microcombs with inverse-designed, meta-dispersion microresonators. *Nat. Photon.* **17**, 943–950 (2023).
103. Zhang, C., Kang, G., Wang, J., Pan, Y. & Qu, J. Inverse design of soliton microcomb based on genetic algorithm and deep learning. *Opt. Express* **30**, 44395–44407 (2022).
104. Pita, J., Nabki, F. & Ménard, M. Inverse-designed silicon nitride reflectors. *Opt. Lett.* **49**, 786–789 (2024).
105. Liu, D., Jiang, R., Bostan, E., Zeng, T. & Yang, K. Nonlinear cavity mode hybridization and dispersion engineering using an inverse-designed mode converter. In *Conf. Lasers Electro Optics* (IEEE, 2025).
106. Mazoukh, C. et al. Genetic algorithm-enhanced microcomb state generation. *Commun. Phys.* **7**, 81 (2024).
107. Jia, Z. et al. Interpretable inverse-designed cavity for on-chip nonlinear photon pair generation. *Optica* **10**, 1529–1534 (2023).
108. Yu, J. et al. Electrically tunable nonlinear polaritonic metasurface. *Nat. Photon.* **16**, 72–78 (2022).
109. Sarma, R. et al. An all-dielectric polaritonic metasurface with a giant nonlinear optical response. *Nano Lett.* **22**, 896–903 (2022).
110. Stich, S. et al. Inverse design of an all-dielectric nonlinear polaritonic metasurface. *ACS Nano* **19**, 17374–17384 (2025).
111. Raju, L. et al. Maximized frequency doubling through the inverse design of nonlinear metamaterials. *ACS Nano* **16**, 3926–3933 (2022).
112. Huang, S.-Y. et al. Multiphoton quantum interference at ultracompact inverse-designed multiport beam splitter. *Opt. Quantum* **3**, 576–582 (2025).
113. Gorshkov, A. V., Calarco, T., Lukin, M. D. & Sørensen, A. S. Photon storage in Λ-type optically dense atomic media. IV. Optimal control using gradient ascent. *Phys. Rev. A* **77**, 043806 (2008).
114. White, A. D., Trivedi, R., Narayanan, K. & Vučković, J. Enhancing superradiance in spectrally inhomogeneous cavity QED systems with dynamic modulation. *ACS Photon.* **9**, 2467–2472 (2022).
115. Mishra, S. D., Trivedi, R., Safavi-Naeini, A. H. & Vučković, J. Control design for inhomogeneous-broadening compensation in single-photon transducers. *Phys. Rev. Appl.* **16**, 044025 (2021).
116. Miguel-Torcal, A., González-Tudela, A., García-Vidal, F. J. & Fernández-Domínguez, A. I. Multiqubit quantum state preparation enabled by topology optimization. *Opt. Quantum* **2**, 371–378 (2024).
117. Bello, M., Platero, G., Cirac, J. I. & González-Tudela, A. Unconventional quantum optics in topological waveguide QED. *Sci. Adv.* **5**, eaaw0297 (2019).
118. Melo, E. G., Eshbaugh, W., Flagg, E. B. & Davanco, M. Multiobjective inverse design of solid-state quantum emitter single-photon sources. *ACS Photon.* **10**, 959–967 (2023).
119. Omirzakhov, K. et al. Single chip 1 Tb/s optical transmitter with inverse designed input and output couplers. Preprint at https://doi.org/10.48550/arXiv.2510.12163 (2025).
120. Alexeev, Y. et al. Artificial intelligence for quantum computing. *Nat. Commun.* **16**, 10829 (2025).
121. Mirhoseini, A. et al. A graph placement methodology for fast chip design. *Nature* **594**, 207–212 (2021).
122. Gil, D. & Moler, K. A. Accelerating science with AI. *Science* **390**, aee0605 (2025).
123. Angeris, G., Vučković, J. & Boyd, S. P. Computational bounds for photonic design. *ACS Photon.* **6**, 1232–1239 (2019).
124. Gertler, S., Kuang, Z., Christie, C., Li, H. & Miller, O. D. Many photonic design problems are sparse QCQPs. *Sci. Adv.* **11**, eadl3237 (2025).
125. Kuang, Z., Miller, D. A. B. & Miller, O. D. Bounds on the coupling strengths of communication channels and their information capacities. *IEEE Trans. Antennas Propag.* **73**, 3959–3974 (2025).
126. Chao, P., Amaolo, A., Molesky, S. & Rodriguez, A. W. Bounds as blueprints: towards optimal and accelerated photonic inverse design. *Opt. Express***34**, 7337–7350 (2026).
127. Mason, S., Ahn, G. H., Grzesik, J., Eun, S. & Vučković, J. High-performance wavelength division multiplexers enabled by co-optimized inverse design. Preprint at https://doi.org/10.48550/arXiv.2509.07233 (2025).

Acknowledgements

The authors acknowledge the financial support from the US Department of Energy ESTEEM Center (to S.M. and G.H.A.), Air Force Office of Scientific Research under award no. FA9550-23-1-0248 (to G.H.A. and L.S.), Advanced Micro Devices through SystemX (to S.M.), Samsung (to S.E. and G.H.A.) and Marvell through SystemX (to S.E.). The authors thank their former team member L. Su for the inverse designs of waveguide bends used in Fig. 1. S.E. acknowledges support from the Shoucheng Zhang Graduate Fellowship and Korea Foundation for Advanced Studies Overseas PhD Fellowship.

Author contributions

The authors contributed equally to all aspects of the article.

Competing interests

J.V. is a cofounder and a scientific adviser of Spins Photonics. S.M., G.H.A. and J.V. are inventors on patent application no. PCT/US2025/036120 (Wavelength division component integrated with distributed Bragg gratings through co-optimization). S.E., G.H.A. and J.V. are inventors on patent application no. PCT/US2025/036482 (Single-mode polarization insensitive grating coupler).

Additional information

Peer review information *Nature Reviews Materials* thanks Owen Miller and Alejandro Rodriguez for their contribution to the peer review of this work.